JOURNAL OF SOLID STATE CHEMISTRY 75, 403–412 (1988)

Optical Transitions of Dy^{3+} Ions in Fluorozirconate Glass

J. L. ADAM, A. D. DOCQ, AND J. LUCAS

Université de Rennes-Beaulieu, Unité Associée au CNRS No. 254, Laboratoire de Chimie Minérale D, Avenue du Général Leclerc, 35042 Rennes Cédex, France

Received December 16, 1987

Optical absorption and emission spectra are presented for Dy^{3+} ions in fluorozirconate (ZBLA) glass. The measured oscillator strengths and radiative rates for several transitions are compared with calculated values. Radiative transition rates for the excited states are determined by using the Judd–Ofelt theory (B. R. Judd, *Phys. Rev.* **127,** 750 (1962); G. S. Ofelt, *J. Chem. Phys.* **37,** 511 (1962)). Thermal evolution of the radiative rate is observed for the $^4F_{9/2}$ level and is well accounted for by Stark level thermalization. Energy transfer effects are responsible for the nonradiative transitions.

Introduction

Easy preparation and good optical properties make fluorozirconate glasses very promising materials for mid-infrared optical fibers and as new hosts for laser applications (*1, 2*). By comparison to oxide glasses, phonon energies as low as 480 cm^{-1} in this fluoride host lead to reduced multiphonon emission rates; this results in a better emission efficiency between *J*-states of the rare-earth ions. In addition, their wide range of transparency, from 250 nm to 6 μm, permits potentially the observation of numerous laser transitions.

The optical properties of several rare-earth ions have already been extensively studied in fluorozirconate glasses. At the moment, data are available for Nd^{3+}, Tb^{3+}, Eu^{2+}, Eu^{3+}, Er^{3+}, Ho^{3+}, Pr^{3+}, and Tm^{3+} ions (*3–16*). The present work adds to these previous reports. Absorption and emission spectra of Dy^{3+} ions in fluorozirconate glasses (ZBLA) are shown. The Judd–Ofelt calculations are carried out in addition to the lifetime measurements.

Experimental

The samples used in this study were of the composition 57 ZrF_4–34 BaF_2–(5-x) LaF_3–4 AlF_3–x DyF_3 where x is equal to 0.1, 0.5, and 2. The method for preparing the glass has been largely discussed in previous reports (*3, 17*) and will not be detailed here.

The absorption spectra were recorded by using a Cary 14 spectrophotometer that operates from 200 nm to 2.5 μm and a Perkin–Elmer 1330 IR spectrophotometer above 2.5 μm. The emission measurements were carried out with light from a 75-W Xenon lamp. The excitation wavelength was selected through a Jobin–Yvon Model H25 monochromator. The emitted light was focused into a Jobin–Yvon HR1000 mono-

0022-4596/88 $3.00

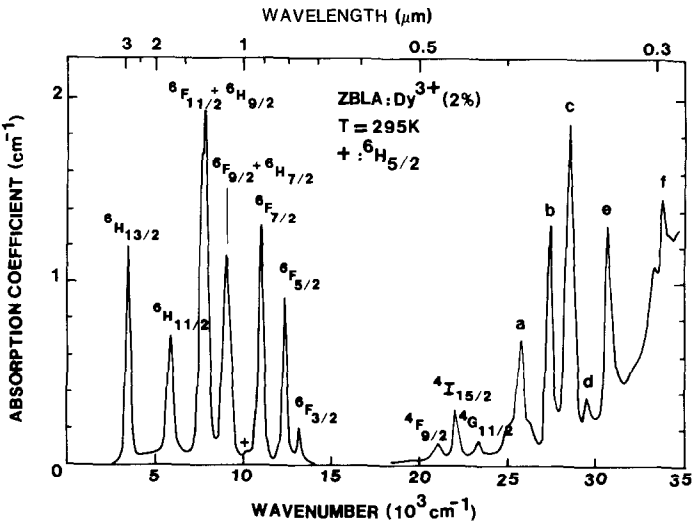

FIG. 1. Absorption spectrum of Dy^{3+} ions in ZBLA glass. Quantum numbers S and L are not well defined for the a–f bands. However, the $^6P_{5/2}$, $^6P_{7/2}$, and $^6P_{3/2}$ states can be reasonably assigned to b, c, and e, respectively (*18*).

chromator and then detected by a Hamamatsu R928S photomultiplier tube. The signal was sent to an EGG Model 128A lock-in amplifier before being displayed on an X–Y recorder. The reference to the lock-in amplifier was a 40-Hz chopper in the excitation beam. The emission intensities were not corrected for instrument response.

Low-temperature measurements were realized by means of a Leybold–Heraeus Model ROK 10-300 cryogenerator controlled by a Variotemp HR1 temperature regulator. Above room temperature, the sample was mounted on a brass holder the temperature of which is controlled by a resistance heater. In practice, temperatures in the range 11–550 K could be achieved.

Lifetimes were measured by using an SRS Model 280 boxcar-averager.

Results

The room-temperature absorption spectrum of ZBLA : Dy^{3+} (2 mole%) is shown in Fig. 1. Transitions in the infrared and the visible are easily assigned. No transition corresponding to the $^6F_{1/2}$ level could be found. Higher energy absorption bands largely overlap, resulting in a loss of accuracy. Previous investigators pointed out that quantum numbers S and L are not reasonably well defined for these levels (*18*). However, most of the energy levels could be determined and the energy diagram is represented in Fig. 2.

The $^4F_{9/2}$ emission spectra in the visible region were recorded at 11, 100, 190 K, and at room temperature. Excitation was at 387 nm into the "a" band. The 11 K and room-temperature spectra are reported in Fig. 3. They clearly show thermalization processes. Weak bands are observable in the high-energy side of the $^4F_{9/2} \rightarrow {}^6H_{15/2}$ and $^4F_{9/2} \rightarrow {}^6H_{13/2}$ transitions at 293 K. They peak at 21,959 and 18,514 cm^{-1}, respectively, and are not present in the lower temperature spectra. These weak bands are undoubtedly due to emission from the $^4I_{15/2}$ level to $^6H_{15/2}$ and $^6H_{13/2}$. Other effects are observable inside the emission bands from $^4F_{9/2}$ to $^6H_{11/2}$, $^6F_{11/2} + {}^6H_{9/2}$, and $^6F_{9/2} +$

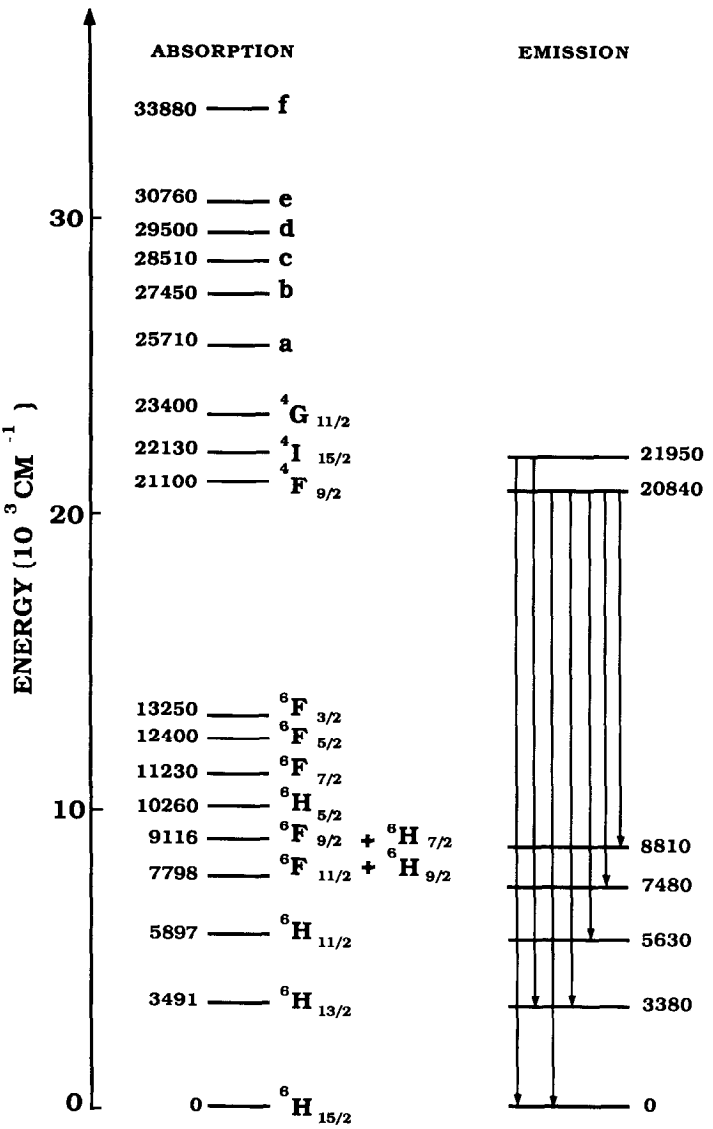

FIG. 2. Energy level diagram of Dy^{3+} ions in ZBLA glass. Levels *a* to *f* are detailed in Fig. 1.

$^6H_{7/2}$, when the temperature is raised above 11 K. They are probably due to thermalization of higher lying sublevels of the $^4F_{9/2}$ state.

Lifetimes were measured as a function of temperature from 11 to 550 K for the $^4F_{9/2} \rightarrow {}^6H_{13/2}$ transition. The results are shown in Table I for a 0.1, 0.5, and a 2% doped sample. In most cases the decay curves could be fitted to single exponentials. Above room temperature, a few measurements were nearly single exponential with a ratio between the first and third *e*-folding times of 0.8. The first *e*-folding time was then chosen as the lifetime. Usually, because of increasing nonradiative rates with temperature, experimental lifetimes decrease when a given sample is warmed

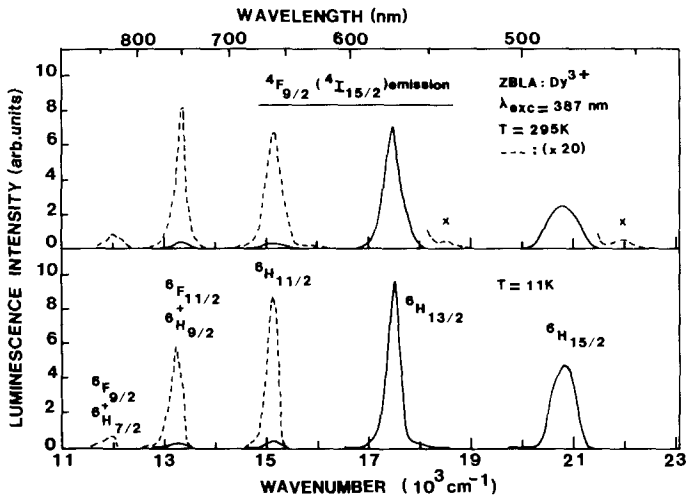

FIG. 3. Emission spectra of Dy^{3+} ions in ZBLA glass from the $^4F_{9/2}$ level. Transitions marked with an x are from the $^4I_{15/2}$ level.

from 11 to 550 K. In our case, the opposite phenomenon is observed at all impurity concentrations. Thermalization processes of higher lying sublevels of the $^4F_{9/2}$ state with longer lifetimes are very likely responsible for that temperature dependence. Unusual behavior of lifetimes versus temperature has been already observed for rare-earth ions in fluorozirconate glasses (*10, 15*) and in crystals (*19*). From the data it is possible to present a fitted curve of the experimental data, assuming sublevel thermalization within the $^4F_{9/2}$ state.

TABLE I

MEASURED $^4F_{9/2}$ EMISSION LIFETIME AS A FUNCTION OF TEMPERATURE AND CONCENTRATION FOR ZBLA : Dy^{3+}

Temperature (K)			Lifetime (μs)		
0.1%	0.5%	2%	0.1%	0.5%	2%
11	11	11	911	765	574
20	20	20	902	762	594
49	51	40	944	784	593
84	80	72	947	812	596
118	110	99	939	817	605
—	141	151	—	844	622
161	170	—	960	816	—
201	199	196	943	849	633
231	231	245	966	836	673
260	260	—	998	841	—
294	295	293	1033	885	662
343	338	353	992	949	696
388	397	398	985	969	701
445	440	445	1063	973	695
493	490	490	1081	1000	698
540	545	537	1025	985	699

Judd–Ofelt Calculations

The oscillator strengths of the absorption bands can be determined experimentally using the following equation:

$$f_{\text{meas}} = \frac{mc}{\pi e^2 N} \int \alpha(\nu) d\nu, \qquad (1)$$

where m and e are the mass and charge of the electron and c is the velocity of light. The number of optically active ions, N, is calculated from the starting glass composition. N is found to be equal to 3.23×10^{20} ions/cm^3 for the 2% doped sample. $\alpha(\nu)$ is the measured absorption coefficient at a given frequency.

The theoretical oscillator strengths are

TABLE II

OSCILLATOR STRENGTHS OF Dy^{3+} IONS IN ZBLA GLASS

Transition	λ (nm)	f_{meas} (10^{-8})	f_{calc} (10^{-8})	Residuals (10^{-8})
$^6H_{15/2} \rightarrow {}^6H_{11/2}$	1696	98	101	−3
$^6F_{11/2}$, $^6H_{9/2}$	1282	365	365	0
$^6F_{9/2}$, $^6F_{7/2}$	1097	218	216	+2
$^6H_{5/2}$	975	7.4	0.6	+6.8
$^6F_{7/2}$	907	181	190	−9
$^6F_{5/2}$	806	108	93	+15
$^6F_{3/2}$	755	26	18	+8
$^4F_{9/2}$	474	15	15	0
$^4I_{15/2}$	452	36	37	−1
$^4G_{11/2}$	427	9.4	4.7	+4.7

Ω_2 (10^{-20} cm^2) = 3.22 rms deviation (10^{-8}) = 8.0
Ω_4 (10^{-20} cm^2) = 1.35
Ω_6 (10^{-20} cm^2) = 2.38

calculated by use of the Judd–Ofelt parameterization (*20, 21*). For an electric dipole transition $SLJ \rightarrow S'L'J'$ of average frequency ν, the calculated oscillator strength is:

$$f_{calc}(J,J') = \frac{8\pi^2 m\nu}{3h} \frac{1}{2J+1} \frac{(n^2+2)^2}{9n} \times \sum_{t=2,4,6} \Omega_t(\langle SLJ| \, |U^{(t)}| \, |S'L'J'\rangle)^2 \quad (2)$$

with

$$n = 1.50583 + \frac{3478.14}{\lambda^2(\text{nm})}, \quad (3)$$

for ZBLA glass. The intensity parameters, Ω_t, are typical of a given ion-host combination. The reduced matrix elements, $U^{(t)}$, are only slightly sensitive to the host. We used the $U^{(t)}$ elements calculated by Carnall for Dy^{3+} aquo and Dy^{3+} in LaF_3 (*22, 23*). In the case of the ($^6F_{11/2}$, $^6H_{9/2}$) and ($^6F_{9/2}$, $^6H_{7/2}$) absorption bands, an appropriate combination of the respective matrix elements is used. All transitions are assumed to be electric dipolar, except for the $^6H_{15/2} \rightarrow {}^6H_{13/2}$ transition which exhibits a nonnegligible magnetic dipolar contribution (*24*). That transition is neglected in the fitting procedure.

The measured and calculated oscillator strengths are listed in Table II. The Judd–Ofelt parameters for the ZBLA–Dy^{3+} combination are found to be $\Omega_2 = 3.22 \times 10^{-20}$ cm^2, $\Omega_4 = 1.35 \times 10^{-20}$ cm^2, and $\Omega_6 = 2.38 \times 10^{-20}$ cm^2. The quality of the fit is given by the root-mean-square deviation which is equal to 8.0×10^{-8}. This value represents a fairly good agreement between measured and calculated oscillator strengths; it is somewhat lower than the rms deviations calculated for ZBLA:Er^{3+} and ZBLA:Ho^{3+} (*10, 12*) and comparable to other Dy^{3+}-doped systems (*25*).

The radiative transition probability for a $SLJ \rightarrow S'L'J'$ electric-dipole emission is calculated from the following equation:

$$A(J;J') = \frac{64\pi^4 e^2}{3(2J+1)h} \frac{1}{\lambda^3} \frac{n(n^2+2)^2}{9} \times \sum_{t=2,4,6} \Omega_t(\langle SLJ| \, |U^{(t)}| \, |S'L'J'\rangle)^2 \quad (4)$$

The total spontaneous emission probability (W_R) for an SLJ excited state is given as the sum of the $A(J;J')$ terms calculated over all terminal states. The radiative lifetime and branching ratios are determined by the following expressions, respectively:

$$\tau_R = \frac{1}{W_R} \quad \text{for an } SLJ \text{ excited state} \quad (5)$$

and

$$\beta = \frac{A(J;J')}{W_R}$$

for an $SLJ \rightarrow S'L'J'$ transition. (6)

For the $^6H_{13/2} \rightarrow {}^6H_{15/2}$ emission, electric plus magnetic dipole, the radiative transition probability is:

$$A(J;J') = \frac{8\pi n^2}{N\lambda^2} \frac{2J'+1}{2J+1} \int \alpha(\nu) d\nu. \quad (7)$$

This relation is obtained by combining Eqs. (1) and (4) extended to electric- and magnetic-dipole transitions. The integral

TABLE III

CALCULATED RADIATIVE TRANSITION PROBABILITIES, RADIATIVE LIFETIMES, AND BRANCHING RATIOS OF Dy^{3+} IN ZBLA GLASS

Transition	λ (nm)	A (sec^{-1})	τ_R (ms)	β
$^6H_{13/2} \rightarrow {}^6H_{15/2}$	2865	19.5	51.2	1.000
$^6H_{11/2} \rightarrow {}^6H_{13/2}$	4156	4.0	13.5[a]	0.052
$^6H_{15/2}$	1696	70.4		0.948
$^4F_{9/2} \rightarrow {}^6F_{1/2}$	1373	0	1.6	0
$^6F_{3/2}$	1280	0		0
$^6F_{5/2}$	1155	3.2		0.005
$^6F_{7/2}$	996	3.0		0.005
$^6H_{5/2}$	923	2.1		0.003
$^6F_{9/2}$, $^6H_{7/2}$	831	15.4		0.026
$^6F_{11/2}$, $^6H_{9/2}$	748	20.2		0.034
$^6H_{11/2}$	658	31.7		0.053
$^6H_{13/2}$	573	371.1		0.615
$^6H_{15/2}$	480	155.8		0.259
$^4I_{15/2} \rightarrow {}^4F_{9/2}$	9709	0.1	2.7	0
$^6F_{1/2}$	1203	0		0
$^6F_{3/2}$	1126	0.3		0.001
$^6F_{5/2}$	1029	0		0
$^6F_{7/2}$	917	0		0
$^6H_{5/2}$	842	0		0
$^6F_{9/2}$, $^6H_{7/2}$	768	10.7		0.029
$^6F_{11/2}$, $^6H_{9/2}$	698	24.1		0.065
$^6H_{11/2}$	616	12.4		0.034
$^6H_{13/2}$	537	42.8		0.116
$^6H_{15/2}$	452	278.6		0.755

[a] The small magnetic-dipole contribution to the $^6H_{11/2} \rightarrow {}^6H_{13/2}$ emission is not taken into account.

term is the integrated absorption coefficient for the $^6H_{15/2} \rightarrow {}^6H_{13/2}$ transition. It is to be noted that the $^6H_{15/2} \rightarrow {}^6H_{13/2}$ absorption band overlaps an O–H absorption band located at 2.9 μm. This is due to the reaction of the glass with the ambient atmosphere during the making procedure. The O–H contribution to the $^6H_{15/2} \rightarrow {}^6H_{13/2}$ integrated absorption coefficient was subtracted before processing Eq. (7). The results are summarized in Table III for the $^6H_{13/2}$, $^6H_{11/2}$, $^4F_{9/2}$, and $^4I_{15/2}$ levels.

Discussion

Despite the very good fit obtained for the Judd–Ofelt parameters calculation (see Table II), the agreement between predicted and measured lifetimes, τ_{calc} and τ_{exp}, is not perfect. The former is equal to 1.6 ms (see Table III) and the latter to nearly 1.1 ms. The experimental value has been determined for the 0.1% doped sample for which no energy transfer between Dy^{3+} ions is expected. Moreover, we have chosen the value obtained at high temperature where a more equal population in the Stark levels of the $^4F_{9/2}$ state brings the experimental conditions closer to the Judd–Ofelt theory requirements. The exclusion of the well-known hypersensitive $^6H_{15/2} \rightarrow (^6F_{11/2} + {}^6H_{9/2})$ transition from the fitting procedure has no dramatic effect on the Judd–Ofeld parameter values. Consequently there is little effect on the predicted radiative lifetimes. The ratio $(\tau_{calc} - \tau_{exp})/\tau_{calc}$ is nearly 30% which is somewhat higher than the established limits of 10–25% (*10*). Nevertheless, valuable information on ZBLA : Dy^{3+} optical properties is still obtainable with this technique.

As reported in Table I, the lifetime data for the $^4F_{9/2}$ level exhibit a general trend to increase with temperature. The radiative emission rate (W_R), multiphonon emission rate (W_{MP}), and energy transfer rate (W_{ET}) account for the observed lifetime according to the following equation:

$$1/\tau_{exp} = W = W_R + W_{MP} + W_{ET}, \quad (8)$$

where W is the total rate (sec^{-1}) for the level in question. From Fig. 2, it can be seen that the energy gap between the $^4F_{9/2}$ level and its next lower lying level ($^6F_{3/2}$) is equal to 7850 cm^{-1}. A negligible multiphonon emission rate is then expected for the emitting level (*15*). For the 0.1% doped sample, the rare-earth ions are supposedly randomly distributed in the glassy host and sufficiently far apart to prevent any Dy^{3+}–Dy^{3+} energy transfer. In consequence, the total rate for the 0.1% sample is equal to the radiative rate and should be temperature independent. Figure 4 portrays

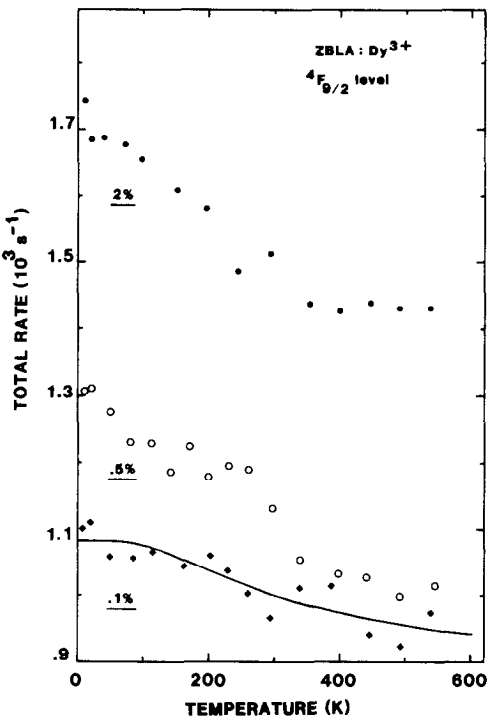

FIG. 4. Total emission rate (W) of the $^4F_{9/2}$ level as a function of temperature for ZBLA : Dy^{3+}.

the plot of the total rates for the 0.1, 0.5, and 2% samples as a function of temperature. The constant line expected for the 0.1% sample is not observed. We have to take into account thermalization processes of higher lying sublevels of the $^4F_{9/2}$ state. Previous investigators pointed out that sublevels radiative rates could be different within a given SLJ state (*10*). The temperature effects observed inside the $^4F_{9/2}$ emission bands support this possibility. The thermalization process for a two-sublevel system may be expressed by the following equation:

$$W_R = \frac{g_1 W_{R1} + g_2 W_{R2} e^{-\Delta E/kT}}{g_1 + g_2 e^{-\Delta E/kT}}, \qquad (9)$$

where W_R is the $^4F_{9/2}$ radiative rate, ΔE is the energy gap between sublevels with radiative rates W_{R1} and W_{R2}, and k is the Boltzman's constant. In this equation, it is assumed that (i) the $(2J + 1)$ sublevels are distributed in two "main sublevels" with degeneracies g_1 and g_2 where $g_1 + g_2 = 2J + 1$, and (ii) the number of emitting ions per second for the $^4F_{9/2}$ state is equal to the sum of emitting ions per second for each "main sublevel." W_{R1}, W_{R2}, and ΔE are determined by a least-square fitting procedure to be the experimental rates shown in Fig. 4 for the 0.1% doped sample. In a glassy material, one cannot predict the degeneracy of perturbed levels for a given state. As a result, Table IV presents data obtained systematically for every combination of (g_1, g_2) as long as $(g_1 + g_2)$ is equal to $(2J + 1)$. The parameters obtained for $g_1 = 1, 2, 8$, or 9 do not agree with physical meaning. Either the energy gap ΔE is equal to ~530 cm^{-1}, which is more than the width at half-maximum (~400 cm^{-1}) for the $^4F_{9/2}$ absorption band, or W_{R2} is found to be negative. These values are not realistic. For $g_1 = 3$ to 7, it is difficult to choose the best set of parameters as the root-mean-square deviation is very similar in all fits. However, it is of importance to point out that theoretical values of W_{R1} and the energy gap ΔE are almost insensitive to the degeneracies distribution when g_1 varies from 3 to 7. As an example, the fitted curve obtained for $g_1 =$

TABLE IV

FITTED PARAMETERS AS A FUNCTION OF DEGENERACIES g_1 AND g_2 IN EQUATION (9), FOR THE $^4F_{9/2}$ LEVEL ($g_1 + g_2 = 2J + 1$)

g_1	g_2	W_{R1} (sec^{-1})	W_{R2} (sec^{-1})	ΔE (cm^{-1})	rms
1	9	1075	894	532	26.8
2	8	1075	813	520	27.9
3	7	1088	855	261	27.4
4	6	1093	808	236	27.8
5	5	1081	663	294	26.2
6	4	1083	562	266	26.2
7	3	1083	320	263	26.2
8	2	1081	−82	253	26.2
9	1	1082	−122	232	26.2

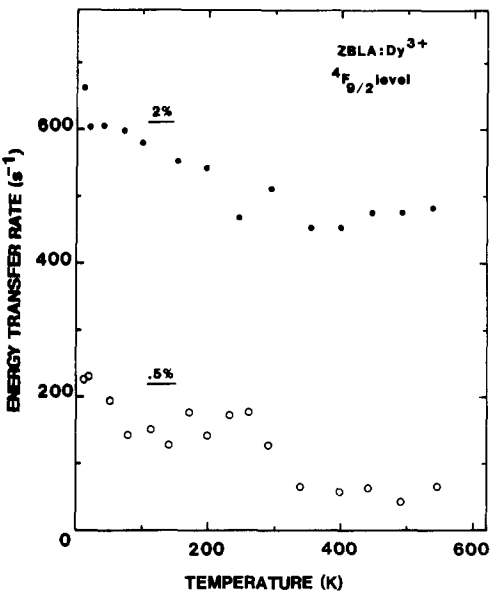

FIG. 5. Energy-transfer rate (W_{ET}) of the $^4F_{9/2}$ level as a function of temperature for ZBLA : Dy^{3+}.

$g_2 = 5$ is presented in Fig. 4 for the 0.1% doped sample. Eq. (9) usually accounts for thermalization effects between SLJ states. We show here that it can be applied to temperature effects inside a given SLJ state. Even though W_{R2} cannot be determined within reasonable limits, Eq. (9) gives valuable information on the energy gap responsible for the thermalization effects.

The data reported in Fig. 4 show that Dy^{3+}–Dy^{3+} energy transfer is present in the 0.5 and 2% samples for the $^4F_{9/2}$ level. It has been pointed out that the multiphonon emission rate is negligible for this level. At a given temperature, by subtracting the total rate of the 0.5 or 2% sample from the fitted curve obtained for the 0.1% sample, the energy transfer rate is found. The results are shown in Fig. 5 as a function of temperature. The usual exponential dependence on inverse temperature (*12, 15*) is not observed. Moreover, one can observe a decrease of the energy transfer rates with temperature which is quite unexpected.

The Forster–Dexter expression for electric dipole–dipole transfer probability is (*26*)

$$P_{dd} = \frac{3\hbar^4 c^4}{4\pi n^4 \tau_S}\left(\frac{1}{R_{SA}}\right)^6 Q_A \int \frac{f_S(E)F_A(E)}{E^4}\,dE, \quad (10)$$

where τ_S is the sensitizer radiative lifetime and Q_A is the activator integrated absorption cross section. The distance between sensitizer and activator is R_{SA}. The normalized line-shape functions for the activator and sensitizer are $F_A(E)$ and $f_S(E)$. The overlap between $F_A(E)$ and $f_S(E)$ is found to be temperature dependent as shown in Fig. 6. This should contribute to increase the transfer probability when the temperature is raised from 11 to 550 K. On the other hand, we have shown that the radiative rate ($1/\tau_S$) decreases with temperature. This

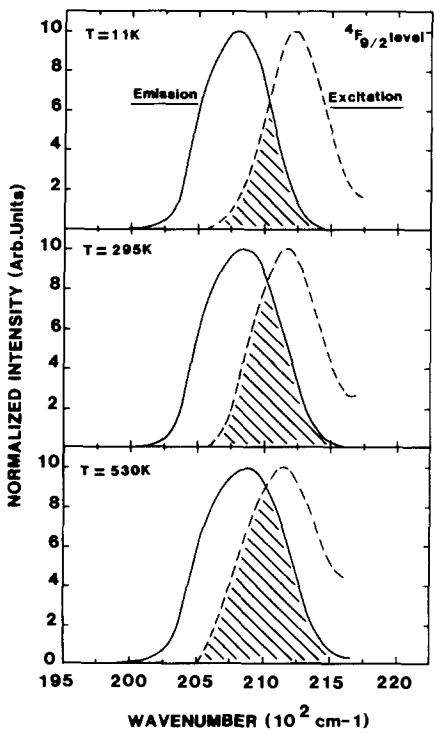

FIG. 6. Emission and excitation overlap of the $^4F_{9/2}$ level as a function of temperature for ZBLA : Dy^{3+}.

phenomenon will decrease the transfer probability and it has to be predominant compared to thermal broadening of emission and excitation bands.

Infrared emissions from the $^6H_{11/2}$ (~1.7 μm) and $^6H_{13/2}$ (~2.9 μm) levels were not investigated. However, their characteristics may be determined from the calculated radiative rates reported in Table III and the multiphonon emission rates calculated by the "energy-gap law" expressed as:

$$W_{MP} = Ce^{-\alpha\Delta E}. \quad (11)$$

The value of constants C and α have been determined previously for ZBLA glass to be $C = 1.88 \times 10^{10}$ sec^{-1} and $\alpha = 5.77 \times 10^{-3}$ cm at 80 K (*10*). The energy gap ΔE is determined from Fig. 2. For the $^6H_{11/2}$ level, the multiphonon emission rate is found to be equal to 17,580 sec^{-1} at 80 K and 29,674 sec^{-1} at 300 K, leading to predicted lifetimes equal to 57 and 34 μsec, respectively. The $^6H_{11/2}$ level is predominantly de-excited by multiphonon emission, whatever the temperature is. Very weak emission is expected, if any. Conversely, for the $^6H_{13/2}$ level, the multiphonon emission rate is 33.6 sec^{-1} at 80 K and 65.7 sec^{-1} at 300 K, leading to predicted lifetimes of 18.8 and 11.7 msec, respectively. Multiphonon emission is still predominant but of the same order of magnitude as radiative emission. Effective emission in the 2.9-μm region may be predicted at liquid nitrogen temperature and at room temperature.

Conclusion

In summary, our experimental results obtained by absorption and emission spectroscopy applied to ZBLA : Dy^{3+} are in agreement with the Judd–Ofelt theory. The lifetime increase with temperature is explained as being due to thermalization of high-energy Stark levels within the $^4F_{9/2}$ emitting state. Dy^{3+}–Dy^{3+} energy transfer is observed even at 0.5% Dy^{3+} concentration and is found to decrease with temperature. Again, Stark level thermalization may be responsible for that. Infrared emission is predicted at 2.9 μm from the $^6H_{13/2}$ level.

References

1. R. Reisfeld, M. Eyal, and C. K. Jorgensen, *J. Less-Common Met.* **126,** 187 (1986).
2. R. C. Powell and W. A. Sibley, *Mater. Sci. Forum* **19–20,** 553(1987).
3. J. Lucas, M. Chanthanasinh, M. Poulain, M. Poulain, P. Brun, and M. J. Weber, *J. Non-Cryst. Solids* **27,** 273 (1978).
4. P. B. Perry, M. W. Shafer, and I. F. Chang, *J. Lumin.* **23,** 261 (1981).
5. W. M. Shafer and P. Perry, *Mater. Res. Bull.* **14,** 899 (1979).
6. B. Blanzat, L. Boehm, C. K. Jorgensen, R. Reisfeld, and N. Spector, *J. Solid State Chem.* **32,** 185 (1980).
7. R. Reisfeld, E. Greenberg, R. N. Brown, M. G. Drexhage, and C. K. Jorgensen, *Chem. Phys. Lett.* **95,** 91 (1983).
8. Xu Gang and R. C. Powell, *J. Appl. Phys.* **57,** 1299 (1984).
9. J. L. Adam, V. Ponçon, J. Lucas, and G. Boulon, *J. Non-Cryst. Solids* **91,** 91 (1987).
10. M. D. Shinn, W. A. Sibley, M. G. Drexhage, and R. N. Brown, *Phys. Rev. B* **27,** 6635 (1983).
11. R. Reisfeld, G. Katz, C. Jacoboni, R. De Pape, M. G. Drexhage, R. N. Brown, and C. K. Jorgensen, *J. Solid State Chem.* **48,** 323 (1983).
12. K. Tanimura, M. D. Shinn, W. A. Sibley, M. G. Drexhage, and R. N. Brown, *Phys. Rev. B* **30,** 2429 (1984).
13. R. Reisfeld, M. Eyal, E. Greenberg, and C. K. Jorgensen, *Chem. Phys. Lett.* **118,** 25 (1985).
14. M. Eyal, E. Greenberg, R. Reisfeld, and N. Spector, *Chem. Phys. Lett.* **117,** 108 (1985).
15. J. L. Adam and W. A. Sibley, *J. Non-Cryst. Solids* **76,** 267 (1985).
16. J. Sanz, R. Cases, and R. Alcala, *J. Non-Cryst. Solids* **93,** 377 (1987).
17. M. Poulain and J. Lucas, *Verres Refract.* **32,** 505 (1978).
18. R. Reisfeld and C. K. Jorgensen, *in* "Handbook on the Physics and Chemistry of Rare-Earths" (K. A. Gschneidner and L. Eyring, Eds.), Chap. 58, pp. 1–90, Elsevier, Amsterdam/New York (1987).
19. J. L. Adam, W. A. Sibley, and D. R. Gabbe, *J. Lumin.* **33,** 391 (1985).
20. B. R. Judd, *Phys. Rev.* **127,** 750 (1962).

21. G. S. OFELT, *J. Chem. Phys.* **37,** 511 (1962).
22. W. T. CARNALL, P. R. FIELDS, AND K. RAJNAK, *J. Chem. Phys.* **49,** 4424 (1968).
23. W. T. CARNALL, H. CROSSWHITE, AND H. M. CROSSWHITE, "Energy Level Structure and Transition Probabilities of the Trivalent Lanthanides in LaF_3," Argonne National Laboratory, Chemistry Division Report (1977).
24. W. T. CARNALL, P. R. FIELDS, AND K. RAJNAK, *J. Chem. Phys.* **49,** 4412 (1968).
25. J. HORMADALY AND R. REISFELD, *J. Non-Cryst. Solids* **30,** 337 (1979).
26. D. L. DEXTER, *J. Chem. Phys.* **21,** 836 (1953).